

## Mass-Ratio Distribution of Hierarchical Triple Systems From the LAMOST-MRS Survey

TONGYU HE,<sup>1,2,3,4</sup> JIANGDAN LI,<sup>5</sup> XUEFEI CHEN,<sup>5</sup> RONG-JIA YANG,<sup>1,2,3,4</sup> LIN XIAO,<sup>1,2,3,4</sup> AND ZHANWEN HAN<sup>5,1</sup>

<sup>1</sup>*College of Physics Science and Technology, Hebei University, Baoding 071002, China*

<sup>2</sup>*Department of Physics, College of Physical Sciences and Technology, Hebei University, Baoding, China*

<sup>3</sup>*Key Laboratory of High-precision Computation and Application of Quantum Field Theory of Hebei Province, Hebei University, Baoding, China*

<sup>4</sup>*Research Center for Computational Physics of Hebei Province, Baoding, 071002, China*

<sup>5</sup>*Yunnan Observatories, Chinese Academy of Sciences (CAS), 396 Yangfangwang, Guandu District, Kunming 650216, P.R. China*

### ABSTRACT

Hierarchical triple-star systems consists of three components organised into an inner binary ( $M_1, M_2$ ) and a more distant outer tertiary ( $M_3$ ) star. The LAMOST Medium-Resolution Spectroscopic Survey (LAMOST-MRS) has offered a great sample for the study of triple system populations. We used the Peak Amplitude Ratio (PAR) method to obtain the mass ratio ( $q_{\text{in}}, q_{\text{out}}$ ) of a triple system from its normalised spectrum. By calculating Cross-Correlation Function (CCF), we determined the correlation between the mass ratio  $q_{\text{out}}$  ( $M_3/(M_1+M_2)$ ) and the amplitude ratio ( $A_3/(A_1+A_2)$ ). We derived  $q_{\text{in}}$  of 0.5–1.0 and  $q_{\text{out}}$  between 0.2 and 0.8. By fitting a power-law function of the corrected  $q_{\text{in}}$  distribution, the  $\gamma_{\text{in}}$  are estimated to be  $-0.654 \pm 2.915$ ,  $4.304 \pm 1.125$  and  $11.371 \pm 1.309$  for A, F and G type stars. The derived  $\gamma_{\text{in}}$ -values increase as the mass decrease, indicating that less massive stars are more likely to have companion stars with similar masses. By fitting a power-law function of the corrected  $q_{\text{out}}$  distribution, the  $\gamma_{\text{out}}$  are estimated to be  $-2.016 \pm 0.172$ ,  $-1.962 \pm 0.853$  and  $-1.238 \pm 0.141$  for G, F and A type stars, respectively. The  $\gamma_{\text{out}}$ -values show a trend of growth toward lower primary star masses.

*Keywords:* Triple stars (1714); Radial velocity (1332)

### 1. INTRODUCTION

Stellar multiplicity is a ubiquitous result of the star formation process, systems with more than two components are quite common in the Universe (Duchêne & Kraus 2013). According to Raghavan et al. (2010a), roughly half of the stars in our Milky Way galaxy are part of binary, triple, or higher order systems. Multi-star systems can provide important information on topics ranging from the formation of a star system, stellar evolution, and galaxy dynamics. Research on stellar multiplicities greater than two, such as triple-star systems, is relatively limited compared to binary systems. Understanding the period distribution, mass ratio and other characteristics of triple-star systems can provide valuable insights into the stellar formation process and stellar evolution. Exploring these systems can help explain the dynamics and interactions within multiple star systems, and contribute to a clearer understanding of stellar evolution and the formation of complex stellar systems (Eggleton & Tokovinin 2008). In the past few decades, there has been an abundance of interesting research on the origin of triple systems. However, exploring the dynamics of triple systems requires solving one of the questions of celestial mechanics: the general three-body problem. It is a triple-star system consisting of three celestial bodies with arbitrary masses and spacings. These bodies can be generally considered as point sources of gravity (Harrington 1977). The study of triple systems is a fascinating subject that involves the interaction and dynamics between three celestial bodies. The gravitational forces between these three bodies can lead to complex and unpredictable motions, making it a challenging problem to solve. Ascertaining the motion in such systems is challenging and hence, researchers rely on observations to discover more triple-star systems. Based on the

increasing sophistication of observational techniques, more and more triple systems are being discovered. Using the Hipparcos catalogue, Eggleton and Tokovinin found that at least 10% of bright stars belong to triple-star (or Multiple-Star) systems (Eggleton & Tokovinin 2008, 2010). Czavalinga et al. (2023) found 376 newly compact hierarchical triple system candidates in their study. They considered that the orbital period is the most trustworthy orbital parameter and that other parameters should be used cautiously. Borkovits et al. (2022) carried out a detailed study of three triple systems in the northern region of TESS and determined their mass, period and RV characteristics. Six new compact triple-star systems were discovered and analyzed by the TESS mission, according to the description in Rappaport et al. (2022). 201 compact hierarchical triple (CHT) systems with outer orbital periods of under 1,000 days were identified in Tokovinin (2018). Kounkel et al. (2021) identified 813 triple candidates in the APOGEE spectra. In addition, Tokovinin (2021) and Toonen et al. (2020, 2022) have reviewed the formation and evolutionary scenarios of the triple system, respectively.

Triple-stars are referred to hierarchical or non-hierarchical structure. Non-hierarchical systems refer to stellar systems that do not have a clear hierarchy or dominance among the triple stars. In these systems, each star is influenced by the gravitational pull of the other stars, but none of them dominate the system. These systems are thought dynamically unstable by Nasab et al. (2023), therefore we only consider hierarchical triple star systems. For example, during the initial mission of the Kepler satellite, Gaulme et al. (2022) discovered KIC 7955301. This is a hierarchical triple system with clear depth and temporal differences in the eclipses. The two white dwarfs are closely connected to each other, orbiting each other. This binary system is joined by a distant red giant orbiting the centre of mass of all three of them.

The hierarchical triple star system consists of three components that are organised into an inner binary pair and a more distant outer star (Czavalinga et al. 2023). To facilitate the application of Kepler’s law, we can approximate the triple as a large orbit (considering the inner binary as a whole and the third star as an outer binary) over a small orbit. For hierarchical triple star systems, we need to take account the stability condition for the existence of the triple systems, which serve as a criterion for the system’s stability. We have picked the most basic formulas through various numerical analyses of the outer to inner binary periods ratio  $P_{\text{out}}/P_{\text{in}}$ <sup>1</sup> (Eggleton & Kiseleva 1995). Equation (1) and equation (2) are pretty straightforward and quite robust.

$$(X_0^{\min})^{2/3} = \left( \frac{1}{1 + q_{\text{out}}} \right)^{1/3} \frac{1 + e_{\text{in}}}{1 - e_{\text{out}}} Y_0^{\min} \quad (1)$$

$$Y_0^{\min} \approx 1 + \frac{3.7}{q_{\text{out}}^{-1/3}} + \frac{2.2}{1 + q_{\text{out}}^{-1/3}} + \frac{1.4}{q_{\text{in}}^{-1/3}} \frac{q_{\text{out}}^{-1/3} - 1}{q_{\text{out}}^{-1/3} + 1} \quad (2)$$

$Y_0^{\min}$  is the critical initial ratio of the outer orbit’s periastron distance to the inner orbit’s apastron distance. The value of  $Y_0^{\min}$  is linked to the critical initial period ratio  $X_0^{\min}$  through the relation shown in equation (1).  $e_{\text{in}}$  and  $e_{\text{out}}$  are the eccentricities of the inner and outer binary in a triple system, respectively.  $q_{\text{in}}$  and  $q_{\text{out}}$  are the inner and outer mass ratios,  $q_{\text{in}} = M_2/M_1 \leq 1$ <sup>2</sup>. We defined  $M_1$ ,  $M_2$  as the inner binary and  $M_3$  as the third star. Due to the limitation of our detection method, our detection efficiency will be very low if the mass of  $M_3$  is greater than the the mass of  $(M_1 + M_2)$ , so we restrict  $q_{\text{out}} = M_3/(M_1 + M_2) \leq 1$ <sup>3</sup>. Moe & Kratter (2018) had considered a triple system with  $q_{\text{out}} > 1$ , the tertiary star ( $M_3$ ) is 1  $M_{\odot}$  and the inner binary  $M_1 = 0.5 M_{\odot}$ ,  $M_2 = 0.4 M_{\odot}$ , but we do not consider this case. In section 5 we demonstrated why this is assumed and demonstrated that the radial velocity (RV) of the third star in most triple systems likely to be located between the RVs of the inner binary stars. These principles are most applicable to triple systems that are nearly co-planar, and our research focuses exclusively on such triple systems. The upper limit for the outer-to-inner period ratio of a stable hierarchical triple star system is around five, according to our estimations thanks to Eggleton’s methods. The smallest outer-to-inner period ratio of the known compact triple system is 5.4 (Xia et al. 2019). Due to the dynamical stability issues in the above equation it is unlikely to find a triple system with a period ratio limit less than 5, so the minimum value of the outer to inner binary period ratio is taken to be 5 in our paper (Offner et al. 2022).

We can study some triple systems by combining information on their orbital parameters, spectra, and photometric measurements. For example, single-line star spectra can be identified because of their variable radial velocities. We

<sup>1</sup>  $P_{\text{out}}$  is the external binary period and  $P_{\text{in}}$  is the internal binary period of a triple system

<sup>2</sup>  $M_1$  is the primary star and  $M_1$  mass is greater than  $M_2$

<sup>3</sup>  $q_{\text{out}} = M_3/(M_1 + M_2) \leq 1$ , because our detection efficiency will be very low if the mass of  $M_3$  is greater than the the mass of  $(M_1 + M_2)$ .

can determine if an object is a multi-star system or not because the spectral lines of its distinct components separate at different radial velocities (RVs). If a target has a triple-line spectrum, it can be considered as a candidate for a spectroscopic triple-star (Li et al. 2021).

In this paper, we have selected main sequence spectroscopic triple (ST) candidates from the LAMOST-MRS spectra given by Li et al. (2021) and investigate the mass-ratio distribution of triple stellar systems. The structure of this paper is as follows. In section 2 We shortly present how the LAMOST-MRS data were selected and classified. In section 3, we introduce the approaches and frameworks applied to the data processing. The results about triple-star systems are shown in Section 4. In section 5 we discuss the completeness of our investigation, comparisons with previous researches, and the significance of the results, and conclusions are given in Sections 6.

## 2. THE DATA

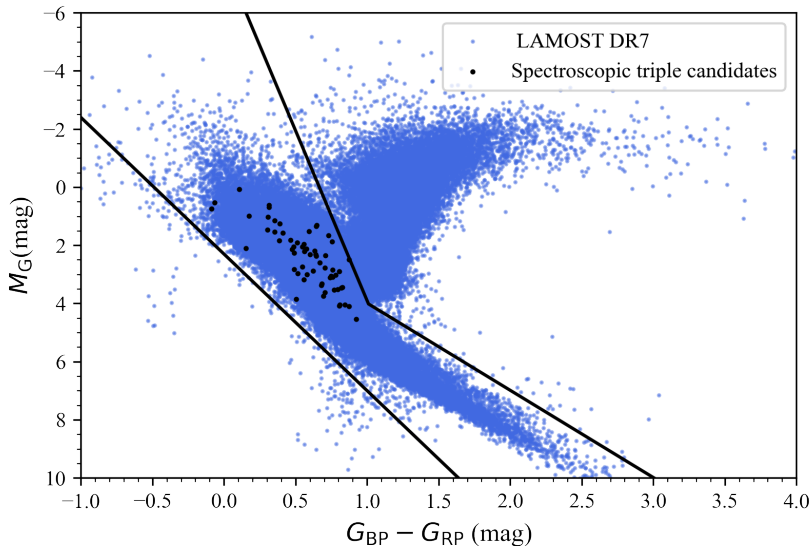


**Figure 1.** The color-magnitude graph of 67 spectroscopic triple (ST) candidates (black dots) determined from LAMOST DR7 data (blue dots). The x-axis shows the colour difference between  $G_{BP}$  and  $G_{RP}$ , and the y-axis displays the absolute value of the  $M_G$ . All photometric data are from *Gaia* DR3, and our samples were chosen between the two lines according to their position on the diagram.

LAMOST is a 4-meter quasi-meridian reflector Schmidt telescope, sited in Hebei province of China. 4,000 fibers are mounted on its 5-degree FoV focal plane, allowing simultaneous observation of 4,000 targets within a 20-square-degree field of view. The LAMOST-MRS red and blue arms have respective wavelength ranges of 6,300 to 6,800Å and 4,950 to 5,350Å. We chose the spectra of the blue arm to detect triple-star candidates and to measure their radial velocity (RV), as they have more absorption lines (Li et al. 2021; Li et al. 2022). Fernandez et al. (2017) found that spectra with low signal-to-noise ratios posed a significant challenge for detecting spectroscopic triple (ST) candidates and Li et al. (2021) chose the blue arm spectra with SNR larger than 10. As a result, the blue arm spectra in LAMOST with SNR higher than 10 were also chosen in our sample.

We applied observations from the LAMOST-MRS spectra of Li et al. (2021) to obtain the mass ratio distribution of spectroscopic triple (ST) candidates. Li et al. (2021) used a cross-correlation function (CCF) and obtained 132 ST candidates from LAMOST-MRS DR7. We cross-matched *Gaia* DR3 with the STs and obtained their magnitudes in the Bp-band, G-band, and Rp-band (Li et al. 2022; *Gaia* Collaboration et al. 2018). Since the diameter of the LAMOST fibre is about 3 arcsec, we used the 3 arcsec search cone to cross-match the spectrum of *Gaia* (Cui et al. 2012). Figure 1 illustrates the colour magnitude map of the ST candidates (black dots). We have corrected the photometric results for the effects of interstellar reddening. We calculated the error in parallax and found that the probability of the error being less than 10% is 86.494%. And all of our samples are in the main-sequence phase and close to the Sun based on Table 1. We used the three-dimensional map of dust reddening from Green et al. (2019). The value of the reddening

**Table 1.** For each spectral type, the number of spectroscopic triple (ST) candidates has been determined

$T_{\text{eff}}$ (K)	SPEC	$N_{\text{all}}$	$N_{\text{ST}}$	$N_{\text{ST}}(500 \text{ pc})$	$N_{\text{ST}}(1000 \text{ pc})$	$N_{\text{ST}}(2000 \text{ pc})$
7200 - 8000	A	9669	7	2	5	7
6000 - 7200	F	58586	35	6	27	34
5150 - 6000	G	76066	20	8	18	20
Total	All	144321	62	16	50	61

NOTE— $N_{\text{ST}}$  is the amount of spectroscopic triple (ST) candidates from the LAMOST-MRS DR7. These ST candidates are sorted into three segments on the basis of  $T_{\text{eff}}$  ranges.  $N_{\text{ST}}$ ,  $N_{\text{ST}}$  and  $N_{\text{ST}}$  display the quantity of spectroscopic triple (ST) candidates within 500 pc, 1000 pc and 2000 pc from the sun, respectively.

factor is taken from Wang & Chen (2019), they derived a table of extinction values of different bands.<sup>4</sup> And we plotted two lines on the figure after visually analyzing the stars’ photometry in the picture. The lower line stands for zero-age MS and the upper line stands for terminal-age MS. We then selected the ST candidates at the position between these two lines in Figure 1 and got a sample of main sequence stages. Finally we got 67 spectroscopic triple (ST) candidates for the main sequence stage.

The essential atmosphere parameters of A and FGK-type stars detected by the LAMOST survey can be automatically determined by LAMOST Stellar Parameter (LASP) (Wu et al. 2014). The main database (MDB) for the LAMOST data processing system is centrally versioned and supported by MySQL. Utilizing the CFI and ULySS algorithms, LASP can perform a two-stage spectral fitting process that efficiently invert the stellar parameters, thereby extracting the stellar parameters of the LAMOST-MRS spectra (Koleva et al. 2009). We utilized the LASP to determine the effective temperature and divide the ST candidates into various spectral types according to the Morgan-Keenan classification (Wu et al. 2011; Luo et al. 2015; Li et al. 2022). Since the spectra of A-type stars are not very sensitive to their temperature, only temperatures below 8,500 K are given. The error values for estimating the effective temperature are typically smaller than 100 K (Li et al. 2022; Wang et al. 2020).

Then we represented the amount of stars for each spectral type and the amount of spectroscopic triple (ST) candidates for each type according to Table 1. Since the effective temperature provided by LASP for late-type stars are unreliable, we excluded stars with temperature below 5,150K. Moreover, we excluded stars with temperature above 8000K to reduce the probability of mixing early-type stars in our ST sample. Therefore, we picked 62 ST candidates of various spectral types. We can see the number of ST candidates at different distance in Table 1.

### 3. METHOD

In this section, we have taken the LAMOST-MRS data and extract the mass ratios of the triple systems. First we generated synthetic spectra by creating simulated triple samples. We then used Merle’s technique to identify multilinear spectral candidates from the spectral samples (Merle et al. 2017). The method that smooth the continuous derivatives of the cross-correlation function (CCF) using a Gaussian kernel. The CCF code is from Zhang et al. (2021). Following this approach, we can identify spectroscopic triple (ST) candidates from synthetic spectra, which exhibit three peaks in their CCF, and we can determine their radial velocities (RVs). Li et al. (2022) discovered a correlation between the mass ratios and Peak Amplitude Ratio (PAR) of spectroscopic binaries (SBs). In the referenced work, the PAR is defined as the ratio between the peak amplitudes of the primary star and secondary star in the CCF, denoted as  $A_1$  and  $A_2$  respectively. However, in our paper, we defined the PAR as the ratio between the peak amplitude of the tertiary star ( $A_3$ ) and the combined peak amplitudes of the inner binary ( $A_2 + A_1$ ). We can apply this method and find a similar relationship between the mass ratios of STs and PAR. By utilizing this relationship, from the PAR displayed in LAMOST-MRS, we can deduce the mass ratios of STs and determine their distribution.

#### 3.1. The CCF method

<sup>4</sup> All EBVs are smaller than 0.6, so we can consider that reddening will have little effect on these triples.

The classical definition of a Cross-Correlation Function(CCF) function about the stellar spectra is:

$$\text{CCF}(h) = \int_{-\infty}^{+\infty} f(x)g(x+h)dx \quad (3)$$

where  $f$  is a normalised spectrum,  $g$  is a normalised template spectrum and  $h$  is the lag expressed in km/s (Merle et al. 2017). The normalized range of the CCF is between -1 and +1, where +1 indicates perfect correlation and -1 indicates perfect anti-correlation.

In this paper, we followed Li et al. (2022) and utilized the normalized solar spectrum of Kurucz (1993) as the template spectrum. The RV range was set from -500 to +500 km/s with a step size of 1 km/s. Some of the peaks in the CCF were too small to be detected, so only the spectra with a peak minimum in the CCF greater than 0.2 were considered. The spectra also need to be normalized prior to analysis.

### 3.2. Construct spectroscopic triples (STs) synthetic spectra

Li et al. (2022) found a relationship between PAR and the mass ratios of SBs. Based on this approach, we found that there should also be some relationships between the mass ratios of spectroscopic triple (ST) candidates and PAR. To test this hypothesis, we have constructed synthetic spectra of triple systems with different temperatures, inner binary mass ratios  $q_{\text{in}}$ , outer binary mass ratios  $q_{\text{out}}$ , radial velocity ( $\Delta RV$ ) and signal-to-noise ratio (SNR) (The stable hierarchical triple stellar system can be thought of as a system of two binary systems, which we here approximate as a large orbit over a small orbit).

To match the LAMOST-MRS spectra, we first created model spectra with a wavelength range of 4,900 Å to 5,400 Å and lowered the resolution from 51,000 to 7,500 by convolution with the laspec code (Zhang et al. 2020, 2021). Then we used the standard value of  $\log g = 4.5$  ( $\text{cm s}^{-2}$ ) for the surface gravity of the main sequence stars, and the metal abundance  $[\text{Fe}/\text{H}]$  was set to 0, the solar metal abundance. Specific information can be found in here Li et al. (2022).

We next built a synthesis spectral lattice of the main-sequence triple system of the solar metal abundance. In the case of MS triple system, all three components are MS stars. By utilizing the effective temperature  $T_{\text{eff1}}$  and logarithmic gravitational acceleration  $\log g$  of the primary star, we have identified a set of data for the main-sequence stars, which include age  $t$ , mass  $M$ , temperature  $T$ , luminosity  $L$ , and other parameters. In order to select simulated spectral ages, it is crucial to control the age range from the zero-age main sequence ( $t = 0$  yr) to the terminal age of the main sequence ( $t = 1.8 \times 10^9$  yr). Additionally, it is important to ensure that all three components of a triple system share the same age. These data can be find from the PARSEC stellar evolution program Li et al. (2022); Bressan et al. (2012).

For a hierarchical triple stellar system, fixing the primary star as  $M_1$  (a constant), we can give the inner binary mass ratio  $q_{\text{in}} = M_2/M_1 \leq 1$ <sup>2</sup>. We have defined  $M_1$  as the primary star because it is the more massive of the inner binary of the triple system.  $q_{\text{out}} = M_3/(M_1 + M_2) \leq 1$ , here we set  $M_1$ ,  $M_2$  as the inner binary and  $M_3$  as the third star<sup>3</sup>. When we identify a primary star as  $M_1$ , it is important to ensure that all three components are main sequence stars of equal age.

Then we interpolated the spectra of the secondary and the third by moving them with a radial velocity difference ( $\Delta RV$ ) and combined the spectra of the secondaries with those of the primary star. We know that identifying spectroscopic triple (ST) candidates relies heavily on the  $\Delta RV$  among the three components. The  $\Delta RV$  between any two components of the three components is a key factor in the identification of ST candidates. It was discovered that the lower limit of the  $\Delta RV$  is 50 km/s, and that this limit is heavily determined by the resolution of the observed spectrum (Li et al. 2022). According to observations made in Li et al. (2021), the maximum  $\Delta RV$  ever detected was 300 km/s. Therefore, any value outside this range has a zero probability of detecting ST candidates. To create a more realistic simulation of the spectra, we introduced Gaussian noise with a targeted signal-to-noise ratio (SNR).

We constructed triple stellar synthetic spectra and hoped to derive the mass ratios distribution ( $q_{\text{in}}$  and  $q_{\text{out}}$ ) of ST candidates from LAMOST-MRS data. To simplify the calculation, we set the gravity of all the components of one triple sysytem to be  $\log g = 4.5$ . Then, with 100 K intervals, we chose the  $T_{\text{eff}}$  of the A-, F- and G-primary stars from 8,000 K to 4,000 K, respectively (Li et al. 2022). These temperature values were chosen because they are characteristic of stars with spectral types of A, F, and G, and are available in the BPS model of Han et al. (2002). Corresponding to the temperature of a primary star, the temperature of these secondary and tertiary stars are also taken at 100 K intervals in the range 4,000-8,000K, but they are always lower than the temperature of the primary star. Here we have used the different temperatures of the three components at the same age in the main sequence phase to correspond

**Table 2.** Parameters for our synthesis spectra grid

Parameter	Value
Wavelength ( Å )	4900 - 5300
Temperature (K)	4000, 4100, 4200, ... , 8000
SNR	10, 20, 50, 100
$\Delta RV$ (km/s)	50, 60, 70, 80, 90, 100, 110, 120, 130, 140, 150
$q_{in}$	0.5, 0.6, 0.7, 0.8, 0.9, 1.0
$q_{out}$	0.2, 0.3, 0.4, 0.5, 0.6, 0.7, 0.8, 0.9, 1.0

NOTE—We have build a lattice of synthetic triple stellar spectra with a resolution of 7,500. Rows 1st, 2nd and 3rd show the wavelength range, effective temperature and signal-to-noise ratio, respectively. Row 4th shows the RV difference of any two components, and rows 5th and 6th show the mass ratios of the inner and outer binaries.

to their mass ratios. For each of the primary star types, we experimented with mass ratios  $q_{in}$  between 0.5 and 1.0, as well as  $q_{out}$  between 0.2 and 1.0<sup>3</sup>. Synthetic spectra were then constructed for triple stars with a given mass ratio and spectral type, using different  $\Delta RV$  and SNR values (refer to Table 2).

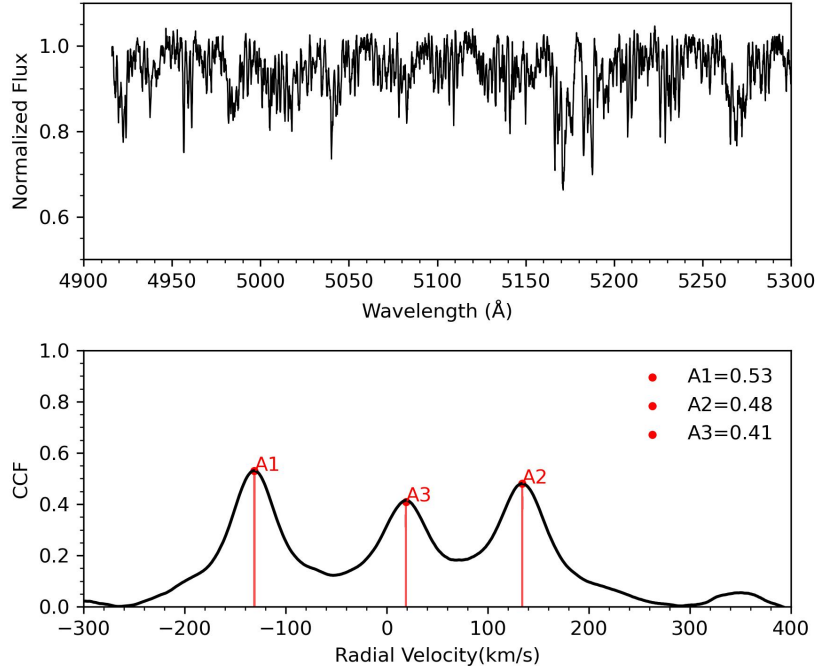


**Figure 2.** An illustration of a triple system’s CCF. In the bottom panel, we display a spectrum of a normalized triple-star system (SNR=20). The effective temperature of three components are  $T_{eff1} = 6,400$  K,  $T_{eff2} = 6,000$  K, and  $T_{eff3} = 5,600$  K. In the lower part of the figure, we present the generated CCF,  $A_1 = 0.53$ ,  $V_1 = -131$  km/s,  $A_2 = 0.48$ ,  $V_2 = 134$  km/s, and  $A_3 = 0.41$ ,  $V_3 = 19$  km/s. The mass ratios are  $q_{in} = 0.96$  and  $q_{out} = 0.441$ , respectively.

We computed the cross-correlation function (CCF) using triple stellar synthetic spectra, Figure 2 displays an example of the CCF calculation. The top portion of Figure 2 displays a triple stellar synthetic spectrum that has been normalized, with effective temperatures of  $T_{eff1} = 6,400$  K,  $T_{eff2} = 6,000$  K and  $T_{eff3} = 5,600$  K. In the lower part of Figure 2 is the generated CCF,  $A_1 = 0.53$ ,  $V_1 = -131$  km/s,  $A_2 = 0.48$ ,  $V_2 = 134$  km/s, and  $A_3 = 0.41$ ,  $V_3 = 19$  km/s.  $A_3$  is the peak amplitude of the tertiary star,  $A_1$  and  $A_2$  are the peak amplitudes of the inner binary, respectively. The

mass ratios are  $q_{\text{in}} = 0.96$  and  $q_{\text{out}} = 0.441$ . The wavelength range considered is between  $4,900 \text{ \AA}$  and  $5,300 \text{ \AA}$ , and the spectral resolution is  $7,500$ . Three peaks are observable, with the left peak representing the amplitude ( $A_1$ ) of the primary star  $M_1$ , the middle peak indicating the amplitude ( $A_3$ ) of the third star  $M_3$ , and the right peak representing the amplitude ( $A_2$ ) of the secondary star  $M_2$ .  $M_1$  is the primary star because it is the more massive of the inner binary ( $M_1, M_2$ ) of the triple system. We can derive  $A_1$  is larger than  $A_2$ ,  $A_3$  is the lowset of the three components.

In Figure 3, when the 1st derivative crosses zero in the falling phase or the 3rd derivative crosses zero in the rising phase, we can determine the number of the three RV components and their values from the triple system (Merle et al. 2017). We noticed that there is more noise in the higher order derivatives of the CCF, minor bumps can occasionally be distinguished as peaks in the CCF. It was necessary to filter the RV range and use the Gaussian filter function `gaussian filter1d` in Python's `scipy.ndimage` package to smooth the derivatives (Virtanen et al. 2020). To select the RV range, two thresholds were employed. The percentile of the CCF is used as the first threshold, while the smoothed second order derivative is used as the second. At the top of Figure 3, we selected 75th percentile of the maximum peak among these three peaks as the threshold. A red line is drawn below this threshold to indicate that peaks below it will not be selected. Similarly, in the third panel of Figure 3, we chose 6th percentile of the maximum peaks among these three peaks as the threshold. A red line is drawn above this threshold to indicate that peaks above it will not be selected. These threshold values were derived from Li et al. (2021).

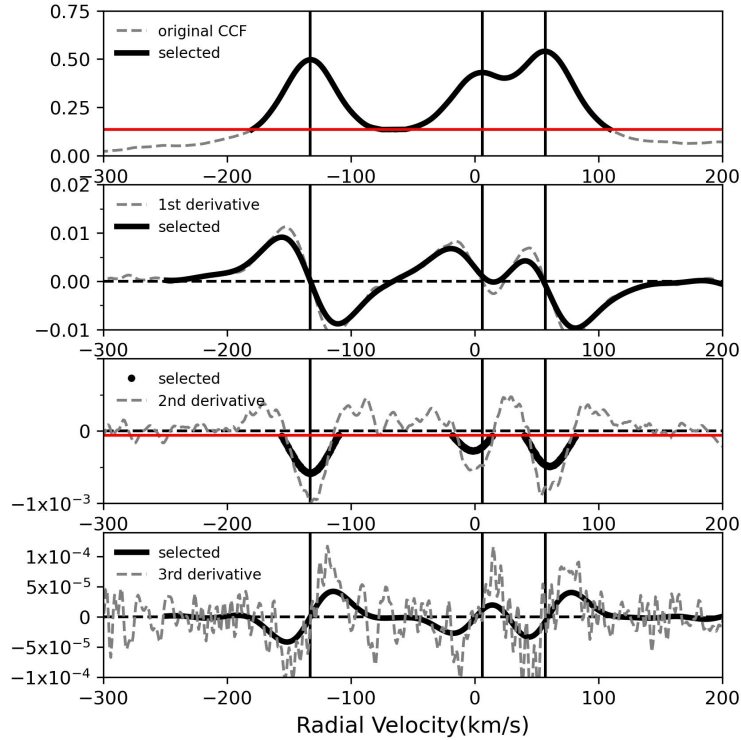


**Figure 3.** CCF and derivatives of one spectroscopic triple (ST) candidate (SNR=20). All the selected range of CCF and smoothed derivatives are shown as black solid lines, while the original CCF and derivatives are shown as gray dashed lines. Each candidate's thresholds are shown as red horizontal lines, their RVs are shown as black vertical lines.

### 3.3. Relationship between mass ratios and amplitude ratios

After constructed synthetic spectra of hierarchical triple systems, we can find the relationship between mass ratios and amplitude ratios. By computing the CCF for all synthetic spectra built for triple systems, we have established the relationship between  $A_3/(A_1 + A_2)$  and  $q_{\text{out}}$ , as well as the relationship between  $A_2/A_1$  and  $q_{\text{in}}$  in Figure 4<sup>5</sup>. For convenience, we have divided these spectroscopic triple (ST) candidates into different types of main sequence stars of

<sup>5</sup>  $A_1$ ,  $A_2$  and  $A_3$  are the primary, secondary and tertiary peak amplitudes

G,F,A according to temperatures of 5600K, 6400K and 8000K. The error bars are the dispersion due to various  $\Delta RV$ s used. In Figure 4 we can see the  $A_2/A_1$  are from 0.37 to 1.0 and the  $q_{in}$  are from 0.5 to 1.0, the  $A_3/(A_1 + A_2)$  are from 0.22 to 0.95 and the  $q_{out}$  are from 0.2 to 1.0. When the  $A_3/(A_1 + A_2)$  is 0.5, the  $q_{out}$  is also 0.5. We have fitted the relationship between  $A_2/A_1$  and  $q_{in}$ , as well as the relationship between  $A_3/(A_1 + A_2)$  and  $q_{out}$  using some functions, as shown in equation (4-9). Using these formulas, we can translate the observed amplitude ratios of the spectroscopic triple candidates into their mass ratios.

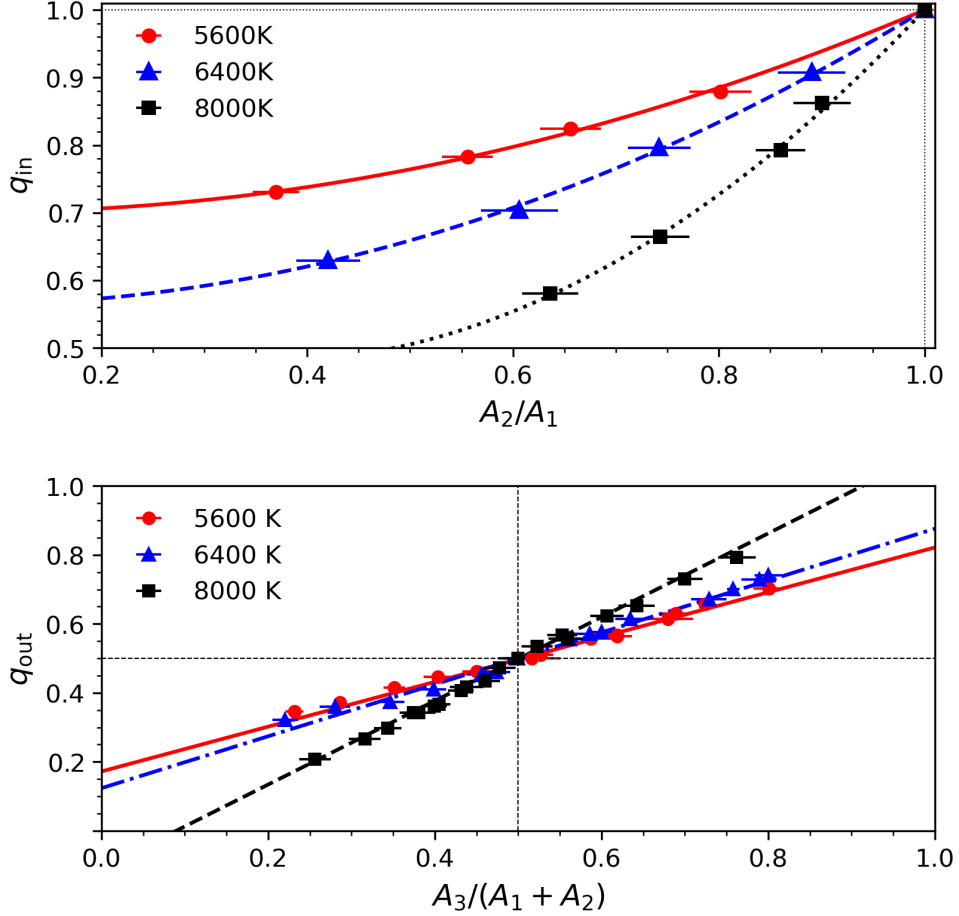


**Figure 4.** Relationship between  $A_2/A_1$  and  $q_{in}$ , as well as the relationship between  $A_3/(A_1 + A_2)$  and  $q_{out}$ . The blue dashed line indicates the result at 6,400 K, the red solid line indicates the relationship at 5,600 K, and the black dashed line indicates the result at 8,000 K.

$$q_{in} = 0.348 \pm 0.044 \times \left(\frac{A_2}{A_1}\right)^2 - 0.051 \pm 0.064 \times \frac{A_2}{A_1} + 0.702 \pm 0.021 \quad (5200\text{K} \leq T_{\text{eff}} \leq 6000\text{K}) \quad (4)$$

$$q_{in} = 0.495 \pm 0.054 \times \left(\frac{A_2}{A_1}\right)^2 - 0.061 \pm 0.082 \times \frac{A_2}{A_1} + 0.566 \pm 0.028 \quad (6000\text{K} \leq T_{\text{eff}} \leq 7200\text{K}) \quad (5)$$

$$q_{in} = 1.256 \pm 0.046 \times \left(\frac{A_2}{A_1}\right)^2 - 0.894 \pm 0.068 \times \frac{A_2}{A_1} + 0.638 \pm 0.023 \quad (7200\text{K} \leq T_{\text{eff}} \leq 8000\text{K}) \quad (6)$$

$$q_{out} = 0.650 \pm 0.011 \times \frac{A_3}{A_1 + A_2} + 0.172 \pm 0.006 \quad (5200\text{K} \leq T_{\text{eff}} \leq 6000\text{K}) \quad (7)$$

$$q_{out} = 0.753 \pm 0.023 \times \frac{A_3}{A_1 + A_2} + 0.123 \pm 0.012 \quad (6000\text{K} \leq T_{\text{eff}} \leq 7200\text{K}) \quad (8)$$

$$q_{out} = 1.214 \pm 0.018 \times \frac{A_3}{A_1 + A_2} - 0.109 \pm 0.008 \quad (7200\text{K} \leq T_{\text{eff}} \leq 8000\text{K}) \quad (9)$$



### 3.4. The spectroscopic triples (STs) detection efficiency

We investigated the spectroscopic triple (ST) detection efficiency to better comprehend how the CCF approach operates and how to rectify the bias in the PAR-derived  $q_{\text{out}}$  distribution. And the detection efficiency is apparent rely on  $q_{\text{out}}$  and  $q_{\text{in}}$ . A triple system with  $q_{\text{in}} > 0.5$  and  $q_{\text{out}}$  from 0.3 to 0.8 can be more easily detected.

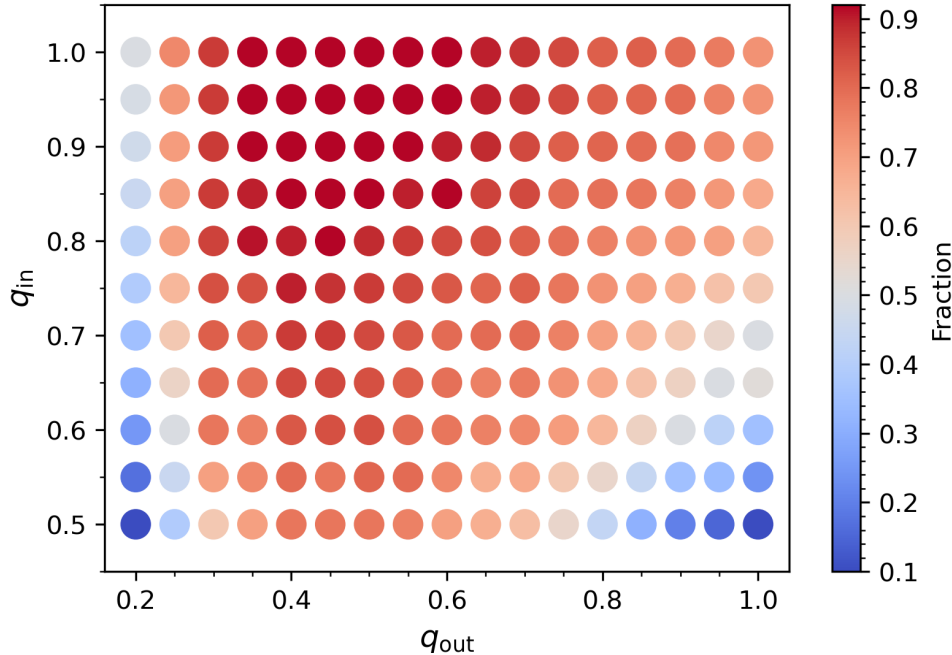


**Figure 5.** Detection efficiency versus mass ratio  $q_{\text{out}}$  and  $q_{\text{in}}$  of spectroscopic triples (STs). The color scale on the right side represents the detection efficiency.

To test the efficiency of the ST detection, we have created a grid of synthetic triplet spectra containing various  $q_{\text{out}}$  and  $q_{\text{in}}$  values. The primaries' effective temperature  $T_{\text{eff1}}$  is assumed to range from 4,000 K to 8,000 K with a step size of 100 K. For a triple system, e.g. Figure 2, there are three radial velocity differences ( $\Delta V$ s), they are  $\Delta V_{1-2}$ ,  $\Delta V_{1-3}$  and  $\Delta V_{3-2}$ . According to the data we obtained from LAMOST in Figure 8, the (left-right) maximum value does not exceed 250 km/s, so we can restrict  $\Delta V_{1-2} \leq 250$  km/s. In addition, we defined  $\Delta V_{\text{min}}$  as the smaller value between  $\Delta V_{1-3}$  (left-middle) and  $\Delta V_{3-2}$  (middle-right), which takes the range of 50 to 125 km/s with a step size of 5 km/s. And we defined  $\Delta V_{\text{max}}$  as the larger value between  $\Delta V_{1-3}$  and  $\Delta V_{3-2}$ , which is larger than  $\Delta V_{\text{min}}$ . With guaranteed  $\Delta V_{1-2} = \Delta V_{1-3} + \Delta V_{3-2} \leq 250$  km/s,  $\Delta V_{\text{max}}$  is also taken with a step size of 5 km/s.

For a triple system, with some parameters such as  $T_{\text{eff1}}$ ,  $\Delta V_{1-2}$ ,  $\Delta V_{2-3}$ ,  $\Delta V_{1-3}$ ,  $q_{\text{in}}$  and  $q_{\text{out}}$ , we can generate 20 spectra with SNR=20, which is a classical value for LAMOST-MRS data. We have examined these spectra using the CCF approach to determine if we can recognize them as STs. The percentage of synthetic spectra that are recognized as STs using the CCF approach is how we determine the detection efficiency. Figure 5 illustrates the detection efficiency of STs for different  $q_{\text{in}}$  and  $q_{\text{out}}$ . We can find the efficiency is large if  $q_{\text{in}}$  is close to 1 and  $q_{\text{out}}$  is from 0.3 to 0.8. The low detection efficiency when  $q_{\text{out}} < 0.3$  is due to that the third's contribution to the triple-star synthetic spectra becomes unimportant when  $q_{\text{out}}$  declines. The low detection efficiency when  $q_{\text{out}} > 0.8$  is due to that the third's contribution to the triple-star synthetic spectra becomes so large that the contribution of the other two components becomes unimportant.

## 4. RESULTS

In section 3.3 we established the relationships between mass ratios ( $q_{\text{out}}, q_{\text{in}}$ ) and amplitude ratios ( $A_3/(A_1 + A_2), A_2/A_1$ ) through several functions. These relationships allowed us to extract information about one component in triple system from LAMOST-MRS spectra. Initially, we have employed the CCFs of the triple stellar spectra to identify some spectroscopic triple (ST) candidates and obtain the amplitude ratios  $A_3/(A_1 + A_2)$  and  $A_2/A_1$  for the

three peaks of the ST candidates (refer to Figure 2). Subsequently, combining the amplitude ratio  $A_3/(A_1 + A_2)$  and  $A_2/A_1$  with these equations derived previously, we estimated the mass ratio  $q_{\text{out}} = M_3/(M_1 + M_2)$  and  $q_{\text{in}} = M_2/M_1$ .

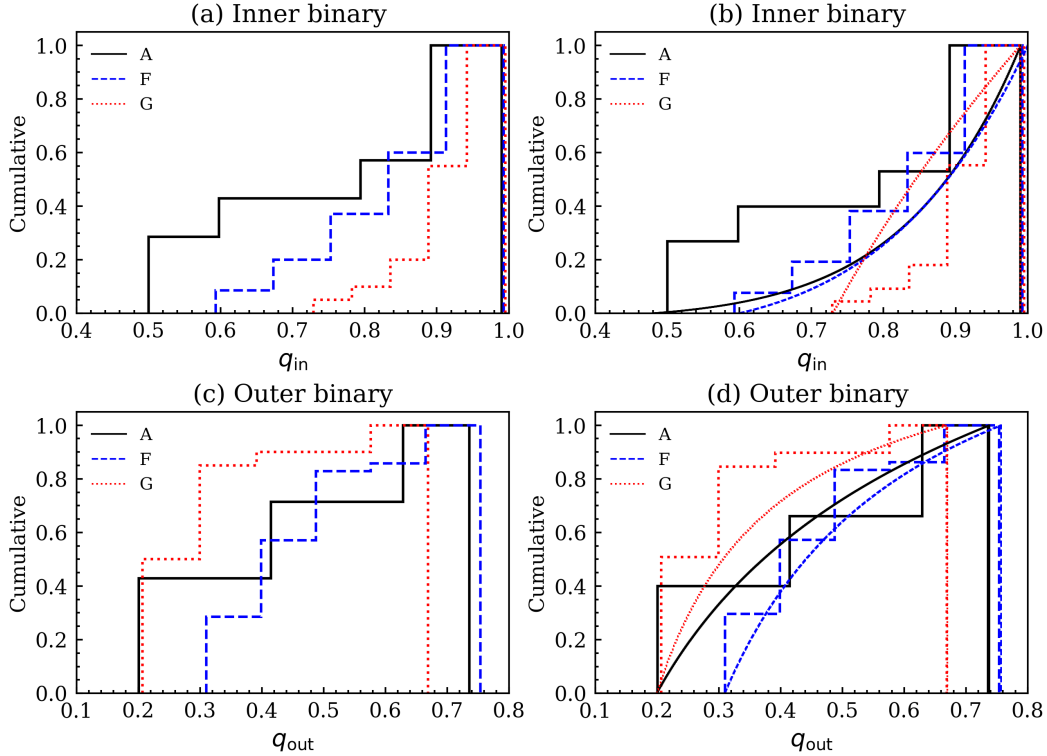


**Figure 6.** The cumulative  $q_{\text{in}}$  and  $q_{\text{out}}$  distribution of triple systems of different spectral types. The  $q_{\text{in}}$  distributions are shown in (a,b), the bias-corrected  $q_{\text{in}}$  distributions and fits are shown in (b). The  $q_{\text{out}}$  distributions are shown in (c,d), and the bias-corrected  $q_{\text{out}}$  distributions and fits are shown in (d).

Based on our assumption that  $M_1$  and  $M_2$  represent the inner binary,  $M_3$  is the third star, we can determine some properties of the triple system. Based on equation (4-9), we have obtained the relation between  $A_2/A_1$  and  $q_{\text{in}}$  (in triple system), and have further obtained the relation between  $q_{\text{out}}$  and the  $A_3/(A_1 + A_2)$  of the triple system. We can also convert the amplitude ratio  $A_2/A_1$  into  $q_{\text{in}} = M_2/M_1$  for inner binary and convert the amplitude ratio  $A_3/(A_1 + A_2)$  into  $q_{\text{out}} = M_3/(M_1 + M_2)$ . Finally we obtained  $q_{\text{in}} = M_2/M_1$ , the mass ratio  $q_{\text{out}} = M_3/(M_1 + M_2)$ , as well as their respective RVs for the triple systems.

We can derive the cumulative  $q_{\text{in}}$  and  $q_{\text{out}}$  distribution of their inner and outer binaries in Figure 6 by investigating the spectra of the 62 spectroscopic triple (ST) candidates. In (a) of Figure 6, we have received the  $q_{\text{in}}$  distribution around the inner binaries. (b) depicts the bias-corrected  $q_{\text{in}}$  distributions using the efficiency of Figure 5. Each triple candidate corresponds to a set of  $q_{\text{in}}$  and  $q_{\text{out}}$  values, which can be found in Figure 5, allowing us to determine the detection efficiency for each candidate. Then, dividing by the detection efficiency can give us the total number of triples, which is the corrected triple count. Based on their different types, they are then categorized as A, F, and G type stars, and finally, their mass ratio distributions are obtained. The bias-corrected  $q_{\text{in}}$  and  $q_{\text{out}}$  distribution, we hypothesized, are all follow the power-law function of  $q^\gamma$ . We then fitted a power-law function to the distribution of corrected  $q_{\text{in}}$  ( $dN/dq_{\text{in}} \propto q_{\text{in}}^{\gamma_{\text{in}}}$ ), the  $\gamma_{\text{in}}$  of  $q_{\text{in}}$  distributions of ST candidate systems are estimated to be  $-0.654 \pm 2.915$ ,  $4.304 \pm 1.125$  and  $11.371 \pm 1.309$  for A, F and G type stars, respectively<sup>6</sup>. We found that there is a large uncertainty in the  $\gamma_{\text{in}}$  values for A-type stars. This could be attributed to a smaller sample size, which led to a rough estimation of the mass ratio distribution. The range of  $q_{\text{in}}$  is from 0.5 to 1.0, and the range of  $q_{\text{out}}$  is from 0.2 to 0.8. The power law exponent  $\gamma_{\text{in}}$  increases as the mass decreases, indicating that less massive stars are more probably to have partner

<sup>6</sup> Given the limited sample size of only 7 A-type stars and the presence of excessively high vsini values, caution must be exercised when interpreting the results of the mass ratio distribution for A-type stars (Section 5.4)

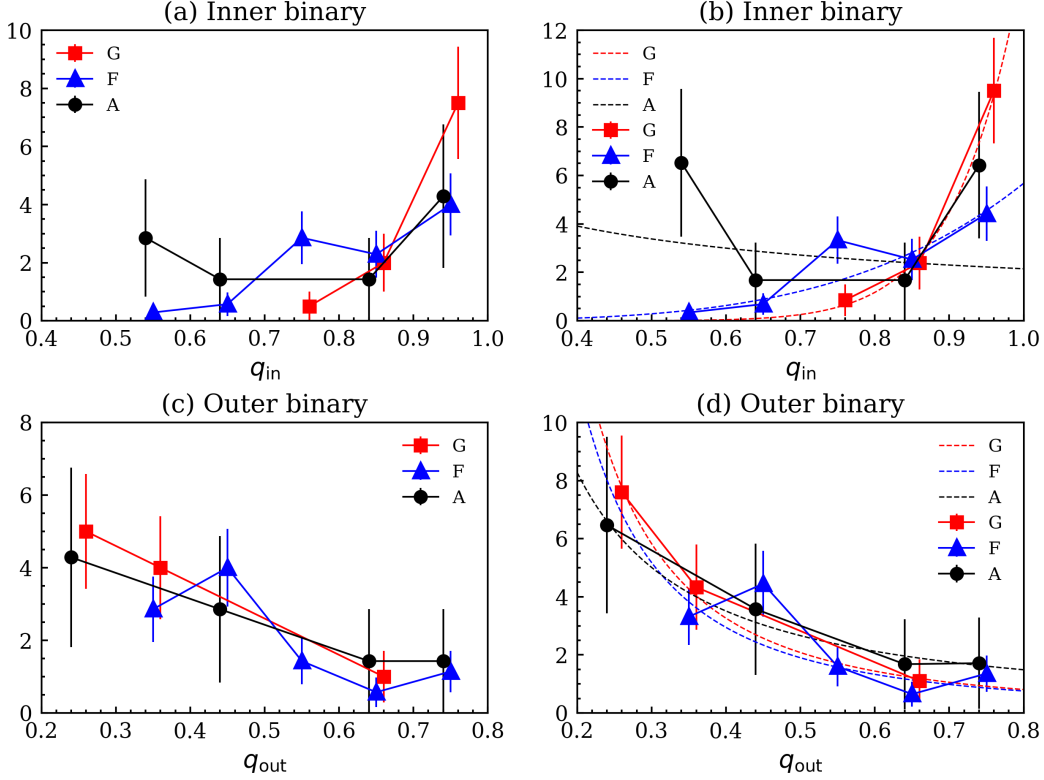


**Figure 7.** The distribution of inner binaries (red squares, black circles, and blue triangles) in triple systems of types A, F, and G are shown in (a,b), the bias-corrected  $q_{in}$  distributions and fits are shown in (b). And (c,d) show the distribution of outer binaries in triple systems in our sample, (d) shows the bias-corrected  $q_{out}$  distributions and fits. In order to clearly show the error bars, we have shifted the mass ratio distribution of A-type stars to the left by 0.1 and the mass ratio distribution of G-type stars to the right by 0.1.

stars with similar masses. Using the efficiency of Figure 5, we also received the  $q_{out}$  distribution about the triple-stars in (b,d) of Figure 6. The (d) depicts the bias-corrected  $q_{out}$  triple distributions. We fitted a power-law distribution to the distribution of the corrected  $q_{out}$  ( $dN/dq_{out} \propto q_{out}^{\gamma_{out}}$ ), the  $\gamma_{out}$  of  $q_{out}$  distributions of ST candidate systems are estimated to be  $-2.016 \pm 0.172$ ,  $-1.962 \pm 0.853$  and  $-1.238 \pm 0.141$  for G, F and A type stars<sup>6</sup>. The  $\gamma_{out}$ -values show a tendency to increase towards lower main star masses.

The distribution of the inner and outer binaries'  $q_{in}$  and  $q_{out}$  are shown in Figure 7. The vertical axis is the density, it is  $dn/dq$ ,  $n$  is the number of the triples,  $q$  is the bin of x-axis,  $bin=0.1$ . In (a,b), we displayed the distribution of inner binaries (red squares, black circles and blue triangles) in triple systems of types A, F and G, the bias-corrected  $q_{in}$  distributions and the fits are shown in (b). The (c,d) show the distribution of outer binaries in triple systems in our sample, the bias-corrected  $q_{out}$  distributions and the fits are shown in (d) (For detailed information, please see Figure 6). The range of  $q_{in}$ , is from 0.5 to 1.0, and the range of  $q_{out}$ , is from 0.2 to 0.8. In Figure 7, (a,b) display that for triple systems the inner binaries tend to be more twin distributions with similar masses, and we can see that the overall trend of the number of ST candidates increase with increasing  $q_{in}$ , and this trend is most obvious in G-type primary stars. While (c,d) show that the number of the third star decreases as  $q_{out}$  increases. However, our method are limited by the mass ratio  $q_{in}$  and  $q_{out}$ . Triple systems can only be efficiently detected in the range  $q_{in}$  of 0.5 – 1.0 and  $q_{out}$  of 0.2 – 0.8.

As a final addition, in Figure 8, we statistically obtained images of the  $\Delta V$  distribution between the any two components of one triple system in the sample. The black dashed line indicates the distance between the left peak and the middle peak ( $\Delta V_{3-2}$ ), the red dashed line indicates the distance between the right peak and the middle peak ( $\Delta V_{1-2}$ ), and the blue dashed line indicates the distance between the left peak and the right peak ( $\Delta V_{1-2}$ ) (refer to 3.4 about the definition of different  $\Delta V$ ). In Figure 8, we found the detected  $\Delta V$  limit is about 50 km/s for ST candidates, which meets the resolution of the LAMOST-MRS spectra. The largest  $\Delta V$  are about 250 km/s for ST

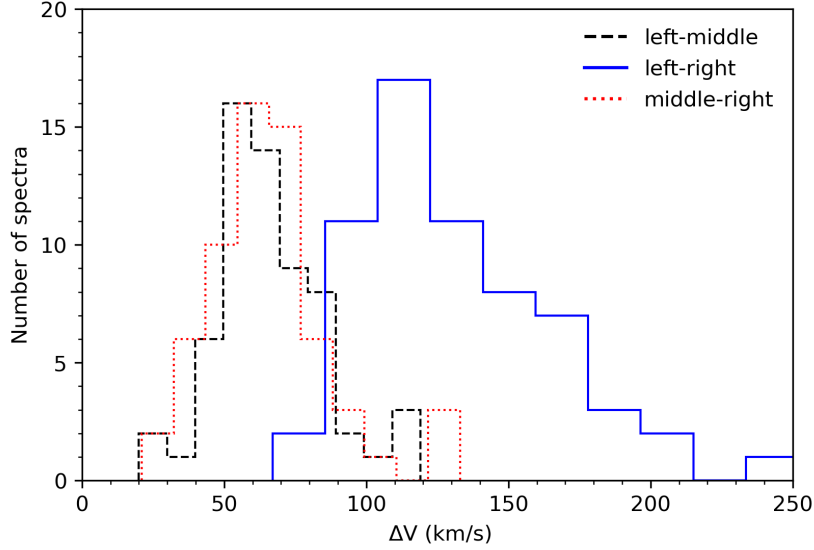


**Figure 8.** Distribution of the number of  $\Delta V$  between any two components in the spectroscopic triple (ST) spectra.

candidates. These observational data can confirm the validity of our selection criteria for radial velocity in section 3.2, which specifies a minimum of 50 km/s and a maximum of 300 km/s. Most of our observational results fall within these ranges. Additionally, the large  $\Delta V$  values represented by the blue line in the graph suggest that inner binary stars in triple systems are all discriminable in our sample using the CCF method (Almost all of the  $\Delta V$ s are large enough). (refer to section 5.1 for more details).

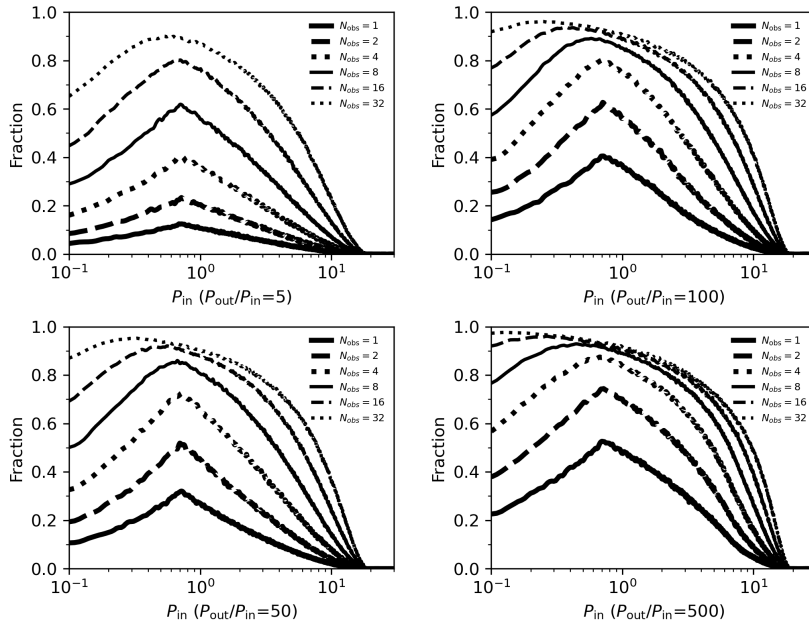


**Figure 9.** Proportion of observed spectroscopic triple (ST) candidates displayed against orbital period for different  $P_{\text{out}}/P_{\text{in}}$  values for a given number of observational epochs. X-axis are the inner binary periods of the triple systems. For 1, 2, and 4 observational epochs, thick solid, dashed, and dotted lines are shown; for 8, 16, and 32 observational epochs, thin solid, dashed, and dotted lines are shown.

## 5. DISCUSSION

### 5.1. The dependence of spectroscopic triple (ST) candidates detection on orbital periods

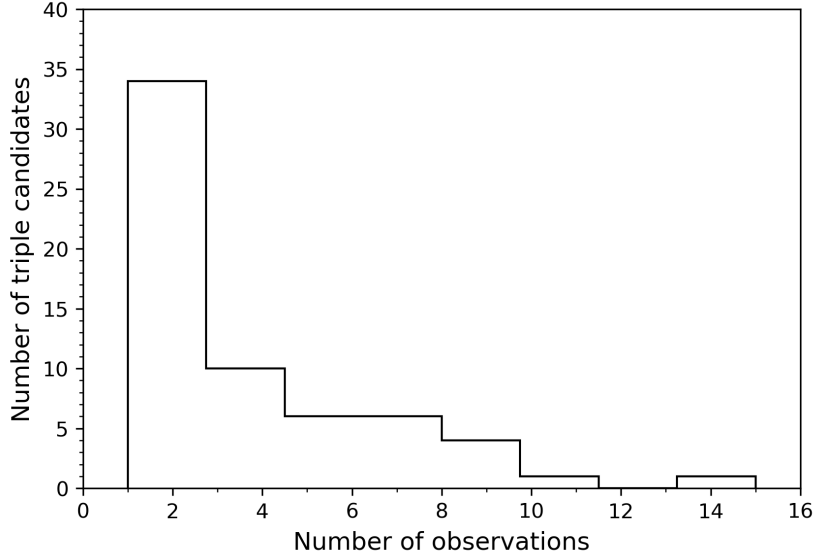


**Figure 10.** Number of the detected spectroscopic triple (ST) candidates versus number of observations.

The orbital period and the number of spectroscopic triple (ST) candidate observed epochs also affect the detection results, and this bias has to be investigated. In Figure 9, we displayed the detection percentage of STs versus orbital period. We assumed that the masses of the primary and the other two components in the triple system are  $1M_{\odot}$ ,  $1M_{\odot}$ , and  $1M_{\odot}$ <sup>7</sup>. The observational epochs are uniformly distributed in orbital phase between 0 and  $2\pi$ , the orbital eccentricity is 0. The inclination range is from 0 to  $2\pi$  and is evenly distributed at solid angles. For a triple system, applying the conditional limit for the existence of a stable hierarchical triple stellar system  $P_{\text{out}}/P_{\text{in}} = 5$  (Eggleton & Kiseleva 1995), we can roughly calculate the  $\Delta V$  between the individual stars of the triple systems by means of Kepler’s law<sup>1</sup>. We gave orbital period  $P_{\text{in}}$  and a number of observational epochs, then we did this calculation for 10,000 triple systems. Li et al. (2022) defined the minimal  $\Delta RV$  about binaries is 50 km/s because the minimal detected  $\Delta RV$  is around 50 km/s from LAMOST-MRS, for triple systems we estimate the minimal  $\Delta V_{1-2}$  is 100 km/s. The detection efficiency is the probability of finding the triple systems with CCF from 10000 simulated samples, corresponding to the vertical coordinate of Figure 9. We defined the detection fraction ratio as the number of (observable) triple systems (the the distance of  $\Delta V_{1-3}$  and  $\Delta V_{3-2}$  are all greater than 50 km/s and less than 300 km/s ,  $\Delta V_{1-2}$  is greater than 100 km/s and less than 300 km/s ) divided by the number of total triple systems.

From Figure 9 we can see that we are able to detect STs orbiting with inner period  $P_{\text{in}}$  of less than 20 days. From the figure we can see that the maximum values of detection efficiency for different number of observational epochs are all in the range of  $P_{\text{in}}$  less than 10 days. In addition the detection efficiency increases slightly as the  $P_{\text{out}}/P_{\text{in}}$  becomes larger. In Figure 9, under the condition where the inner binary period in a triple system is less than 20 days, we can estimate the detection probabilities of the triple systems types A, F, and G to be 7.9 ‰, 5.0 ‰ and 2.6 ‰, respectively<sup>8</sup>. However there are some limitations about our estimates. With only seven A-type stars in our sample and their rapid axial rotation, the detection efficiency in identifying A-type star triple systems may be significantly lower than our previous predictions, with a reduction by a factor of approximately four. For more details, see 5.4. The majority number of observations in Figure 10, are less than 5, indicating that the triple systems we are currently able to detect represent (13.95%) is a very small fraction of the triple systems.

### 5.2. Probability that the RV of the third star is in the middle of the inner binary (a triple stellar system)

<sup>7</sup> We can choose different qualities, which does not affect the result.

<sup>8</sup> We estimated the probability of A, F, G-type stars in triples at different outer-to-inner period ratios ( $P_{\text{out}}/P_{\text{in}}$ ) and found that the results did not differ much, we finally chose the result with  $P_{\text{out}}/P_{\text{in}} = 50$ .

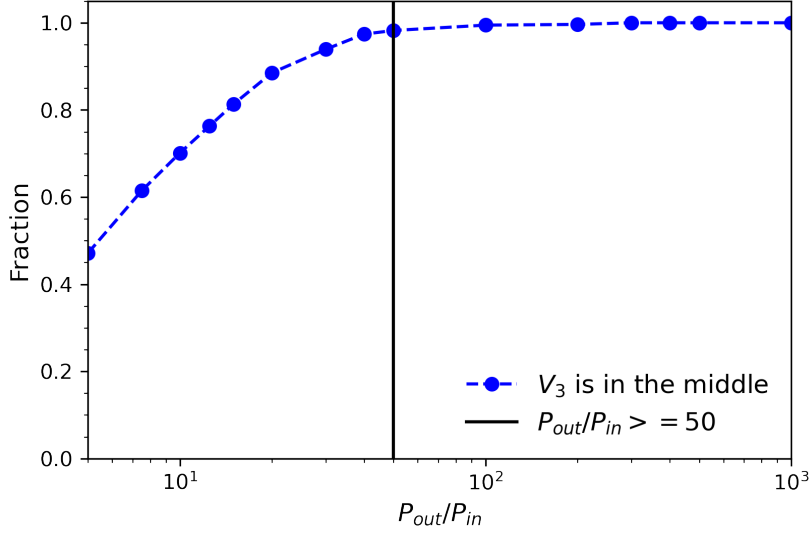


**Figure 11.** The probability that the RV of the third star ( $M_3$ ) is in the middle of the inner binary ( $M_1, M_2$ ) for hierarchical triple systems. The black line represents the value of the inner to outer period ratio ( $P_{out}/P_{in}$ ) is greater than 50.

Our previous argument was based on the assumption that  $V_3$  is located between  $V_1$  and  $V_2$  (the inner binary) for a stable hierarchical triple system with  $M_1$  and  $M_2$  as the inner binary and  $M_3$  as the tertiary star. We can prove that  $V_3$  is mostly located between  $V_1$  and  $V_2$ . We assumed that the masses of the primary star, secondary star, and third star are all  $1M_{\odot}$ , which is consistent with section 5.1. We randomly selected 10000 triple systems, we defined the detection fraction as the number of cases where  $V_3$  is in the middle of  $V_1$  and  $V_2$  (and the distance of  $\Delta V_{1-3}$  and  $\Delta V_{3-2}$  are all greater than 50 km/s and less than 300 km/s,  $\Delta V_{1-2}$  is greater than 100 km/s and less than 300 km/s) divided by the total number of cases where the distance between any two of  $\Delta V_{1-2}$ ,  $\Delta V_{3-2}$ , and  $\Delta V_{1-3}$  is greater than 50 km/s and less than 300 km/s (refer to section 5.1 for more details).

Figure 11 shows the probability of  $V_3$  being located between  $V_1$  and  $V_2$  for different values of the outer-to-inner period ratio  $P_{out}/P_{in}$  in triple systems. We found that as the value of  $P_{out}/P_{in}$  increased, the probability that  $V_3$  is located between  $V_1$  and  $V_2$  gradually approached 1. The black line represents the minimum value of the outer-to-inner period ratio ( $P_{out}/P_{in}$ ) obtained from our simulations with the 62 ST candidates.

First, we utilized Kepler's laws to establish a relationship between the outer-to-inner period ratio ( $P_{out}/P_{in}$ ) and the three radial velocities (RVs). To simplify the triple system problem, we treated it as two binary systems. Let  $m$  represent the total mass of the inner binary,  $M$  denote the total mass of all three components,  $t$  represent the period of the inner binary, and  $T$  indicate the outer orbital period. Additionally,  $r_2$  signifies the distance of the inner binary, while  $r_1$  is the distance of the tertiary star from the center of the inner binary (approximation).  $\phi$  is the phase and  $i$  is the inclination. The formulas used were as follows:

$$M = m_1 + m_2 + m_3, m = m_1 + m_2 \quad (10)$$

$$r_1 = \sqrt[3]{\frac{GMT^2}{4\pi^2}}, r_2 = \sqrt[3]{\frac{Gmt^2}{4\pi^2}} \quad (11)$$

$$V_1 = \frac{2\pi}{t} r_2 \frac{m_2}{m_1 + m_2} \sin\phi \sin i, V_2 = \frac{2\pi}{t} r_2 \frac{m_1}{m_1 + m_2} \sin\phi \sin i \quad (12)$$

$$V_3 = \frac{2\pi}{T} r_1 \frac{m_1 + m_2}{m_1 + m_2 + m_3} \sin\phi \sin i \quad (13)$$

We can finally derive:

$$P_{out}/P_{in} = \frac{T}{t} \propto \frac{\Delta V_{1-2}^3}{(V_3 - \frac{V_1+V_2}{2})^3} \quad (14)$$

In section 3.2, we already obtain the radial velocities of each component. Bringing the different  $V$ s into the formulas, we can roughly estimate to get the ratio  $P_{out}/P_{in}$  of these 62 triple candidates. We put a black line in Figure 11,

which means most of the triples in our sample have  $P_{\text{out}}/P_{\text{in}}$  greater than 50. And corresponding to Figure 11, we can find that with  $P_{\text{out}}/P_{\text{in}}$  greater than 50, the tertiary star's  $V_3$  has a 95 % probability of being in the middle of  $V_1$  and  $V_2$ . This suggests that our previous hypothesis is reasonable. In recent years, Czavalinga et al. (2023) summarized the inner and outer periods of some discovered triple systems and found that most of the inner binary periods are less than 10 days while most of the outer periods are larger than 300 days, which further confirms the validity of our hypothesis for most triple systems.

### 5.3. Multiple observations

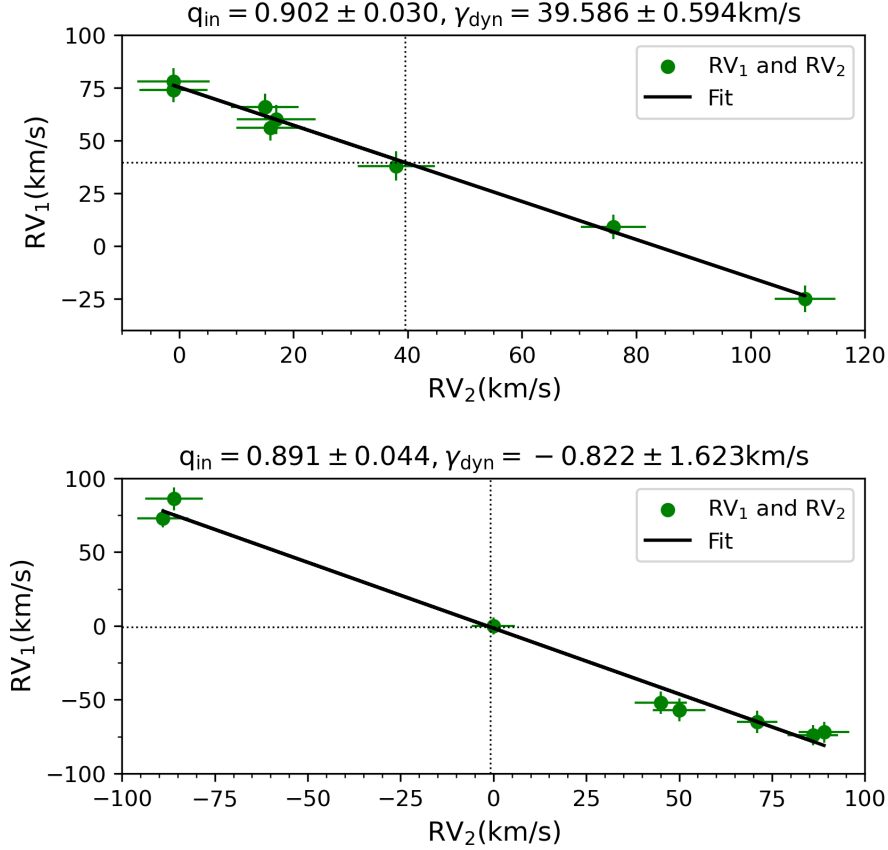


**Figure 12.** The coordinates of the triple candidate depicted in the upper part are RA=134.1496 and DEC=12.59047, while the coordinates of the triple candidate illustrated in the lower part are RA=292.718 and DEC=41.922. The x-axis is the  $RV_1$  and the y-axis is the  $RV_2$ . The black line represents the fitted equation, with the parameters listed in the title. The intersection points of the two black dashed lines represent the systemic velocities  $\gamma_{\text{dyn}}$ .

In this section, we discussed the results obtained by analyzing multiple observations of several triple candidates that had a high number of observations in Figure 10. We specifically counted these multiple observations in order to extract information about their mass ratios from the changes observed in their radial velocities (RVs).

Figure 12 illustrates two examples where we obtained multiple measurements of  $RV_1$  and  $RV_2$ . Utilizing this equation:  $RV_1 = \gamma_{\text{dyn}}(1 + q_{\text{in}}) - q_{\text{in}}RV_2$ , we can determine the mass ratio ( $q_{\text{in}}$ ) and systemic velocity ( $\gamma_{\text{dyn}}$ ) of the inner binary (Wilson 1941; Kovalev et al. 2022). The parameters obtained from the linear fitting in the upper part of Figure 12 are as follows:  $q_{\text{in}} = 0.902 \pm 0.030$ ,  $\gamma_{\text{dyn}} = 39.586 \pm 0.594 \text{ km/s}$ , and the results obtained from the CCF is  $q_{\text{in}} = 0.881 \pm 0.138$ <sup>9</sup>. The parameters obtained from the lower part are as follows:  $q_{\text{in}} = 0.891 \pm 0.044$ ,  $\gamma_{\text{dyn}} = -0.822 \pm 1.623 \text{ km/s}$ , and

<sup>9</sup> We obtained the results of the CCF analysis based on one selected spectrum.

the results obtained from the CCF is  $q_{\text{in}} = 0.872 \pm 0.136$ <sup>9</sup>. The fact that these results fall within the range of error indicates that our method is valid and reliable, and our method does not rely on multiple observations.<sup>10</sup>

#### 5.4. Comparison with previous Work

In Li et al. (2022)’s work, they came up with a PAR method to calculate mass ratios from PARs of CCFs between the spectra of binaries and the solar spectrum. Type-G binaries are more likely to be twins, according to their analysis of the mass ratio distribution. For orbital periods less than 155 d and mass ratios greater than 0.6, the binary fractions for A, F and G stars are  $7.6 \pm 0.5\%$ ,  $4.9 \pm 0.2\%$  and  $3.7 \pm 0.1\%$ , respectively.

In our work, we estimated the fractions of the hierarchical triple systems A, F, and G to be 7.9 ‰, 5.0 ‰ and 2.6 ‰, respectively. Note that the derived mass ratio distribution and the proportion of triple systems mentioned here specifically apply to triple systems with an inner period ( $P_{\text{in}}$ ) shorter than 20 days, an inner mass ratio ( $q_{\text{in}}$ ) higher than 0.5, and an outer mass ratio ( $q_{\text{out}}$ ) higher than 0.2. The rapid axial rotation of the A-type stars can indeed have an impact on spectral analysis. Royer et al. (2007) used the whole profile of Fourier transform of spectral lines to derive the  $v \sin i$ , and the corresponding  $v \sin i$  values for different classes of stars are extensively presented in their work. Our sample of A-type stars all have temperatures below 8,000K and we can find that the median value of  $v \sin i$  is 125km/s in Royer et al. (2007)’s work.

We constructed a batch of triple spectra with  $v \sin i$  values of 125 km/s (the temperature of A-type stars to be 8,000K,  $\log g = 4.5$ , metal abundance [Fe/H] set to 0). And we made a rough estimate of the mass ratio distribution ( $q_{\text{in}}$  and  $q_{\text{out}}$ ). The results are very similar to those in Figure 4 for the temperature of 8,000 K. We found that the rotation of A-type stars has little effect on the mass ratio distribution of  $q_{\text{in}}$  and  $q_{\text{out}}$ . This is because we are primarily interested in the amplitude ratios  $A_2/A_1$  and  $A_3/(A_1 + A_2)$  within the triple systems, rather than the individual amplitudes of each component. And in our sample of A-type stars, almost all the  $\Delta RV$  are less than 125 km/s. The lower the rotational velocity of A-type stars, the higher our detection efficiency. Furthermore, we utilized Kepler’s law to roughly estimate the  $v \sin i$  of A-type binary stars with periods less than ten days and found that the most values are lower than 125 km/s. This indicates that the  $v \sin i$  values of A-type stars in multiple star systems are generally lower than those of single A-type stars.

$\log P$  is the simplest and most commonly used form, assuming  $\log P$  can conveniently describe and analyze the multiplicity of stars. Raghavan et al. (2010b) provided observational evidence, and later Duchêne & Kraus (2013) and Moe & Kratter (2018) also used the  $\log P$  assumptions. We compared the inferences we estimated with Li et al. (2022)’s binary fraction, and we found that our estimated proportion of triples is about 1/5 of the proportion of their binaries. The  $P_{\text{in}}$  in our triples are all less than 20 days, which indicates that inner binaries are relatively close together and mass transfer are likely to occur in them. Based on Toonen et al. (2020), the triple system’s inner binary’s initially most massive star fills its Roche lobe and begins transferring mass to its companion. In their sample, 63–74% of the triple systems experienced this, while some triples (2–4.5%) experienced dynamic instability during their evolution. Furthermore, according to Kummer et al. (2023), mass transfer occurs in the inner binary of the vast majority of massive triple stars (65–77%), which is different from isolated binary development, where mass transfer occurs less frequently. Our study of  $q_{\text{out}}$  suggests that the tertiary stars in triple systems have little to do with inner binaries. In addition, because the inner binaries of triples tend to be more compact compared to isolated binaries, the probability of mass transfer occurring in triples are greater than in isolated binaries (Toonen et al. 2020). By studying triple-star systems, we can gain a deeper understanding of the evolutionary processes, internal structures, and behavioral characteristics of stars in the universe. This knowledge is significant in helping us comprehend the mechanisms involved in star formation and evolution.

## 6. CONCLUSIONS

In this paper, we utilized the peak amplitude ratio (PAR) approach to determine mass ratios from the cross-correlation function (CCF) between triple stellar spectra and the binary spectra (Li et al. 2022). We subsequently investigated the mass ratios distribution using this approach with the LAMOST-MRS data.

We obtained some equations that describe the relationships between mass ratios and amplitude ratios of triple stellar systems. Using these equations, we can derive information about the masses and radial velocities of triple systems,

<sup>10</sup> The mass ratio results we obtained are slightly smaller, which may be due to the fact that as the signal-to-noise ratio increases, the peak obtained from the CCF becomes higher.



which can aid in more thorough investigations of spectroscopic triple (ST) candidates. We identified 62 main-sequence ST candidates and categorized them as A, F and G-type stars to further analyze their distribution characteristics.

We fitted a power-law function to the distribution of corrected  $q_{\text{in}}$  ( $dN/dq_{\text{in}} \propto q_{\text{in}}^{\gamma_{\text{in}}}$ ), the  $\gamma_{\text{in}}$  of  $q_{\text{in}}$  distributions of ST candidate systems are estimated to be  $-0.654 \pm 2.915$ ,  $4.304 \pm 1.125$  and  $11.371 \pm 1.309$  for A, F and G type stars, respectively. The power law exponent  $\gamma_{\text{in}}$  increases as the mass decreases, indicating that less massive stars are more likely to have partner stars with similar masses. We have found that the inner binaries in triple systems tend to have more similar mass combination, and this trend is most obvious in G-type primary stars. We also fitted a power-law distribution to the distribution of the corrected  $q_{\text{out}}$  ( $dN/dq_{\text{out}} \propto q_{\text{out}}^{\gamma_{\text{out}}}$ ), the  $\gamma_{\text{out}}$  are estimated to be  $-2.016 \pm 0.172$ ,  $-1.962 \pm 0.853$  and  $-1.238 \pm 0.141$  for G, F and A type stars, respectively. The  $\gamma_{\text{out}}$ -values show a tendency to increase towards lower main star masses. Under the condition where the inner binary period in a triple system is less than 20 days ( $\log P$  is uniformly distributed) and the masses of the three components do not vary significantly ( $q_{\text{in}} > 0.5$ ,  $0.8 > q_{\text{out}} > 0.2$ ), we can estimate (imprecise) the probabilities of the triple systems A, F, and G to be 7.9 ‰, 5.0 ‰ and 2.6 ‰, providing information for further study of the distribution of triple systems<sup>6</sup>.

#### ACKNOWLEDGMENTS

We thank Lihuan Yu, Jiao Li, Qida Li, Qiyuan Cheng, and Zhenwei Li for their helpful insights. This work was in part supported by the National Natural Science Foundation of China under Grant Nos.12288102, 12090040/3, the National Key R&D Program of China under Grant No.2021YFA1600400/1, and the International Center of Supernova, Yunnan Key Laboratory under Grant No.202201BC070003. Guoshoujing Telescope (LAMOST) is a National Major Scientific Project built by the Chinese Academy of Sciences. Funding for the project has been provided by the National Development and Reform Commission. LAMOST is operated and managed by the National Astronomical Observatories, Chinese Academy of Sciences. This work has made use of data from the European Space Agency (ESA) mission Gaia (<https://www.cosmos.esa.int/gaia>), processed by the Gaia Data Processing and Analysis Consortium (DPAC, <https://www.cosmos.esa.int/web/gaia/dpac/consortium>).

*Software:* LASP pipeline (Wu et al. 2011; Luo et al. 2015) ULySS (Koleva et al. 2009) SPECTRUM (Gray & Corbally 1994) laspec (Zhang et al. 2020, 2021)

#### REFERENCES

- Borkovits, T., Mitnyan, T., Rappaport, S. A., et al. 2022, MNRAS, 510, 1352, doi: [10.1093/mnras/stab3397](https://doi.org/10.1093/mnras/stab3397)
- Bressan, A., Marigo, P., Girardi, L., et al. 2012, MNRAS, 427, 127, doi: [10.1111/j.1365-2966.2012.21948.x](https://doi.org/10.1111/j.1365-2966.2012.21948.x)
- Cui, X.-Q., Zhao, Y.-H., Chu, Y.-Q., et al. 2012, Research in Astronomy and Astrophysics, 12, 1197, doi: [10.1088/1674-4527/12/9/003](https://doi.org/10.1088/1674-4527/12/9/003)
- Czavalinga, D. R., Mitnyan, T., Rappaport, S. A., et al. 2023, A&A, 670, A75, doi: [10.1051/0004-6361/202245300](https://doi.org/10.1051/0004-6361/202245300)
- Duchêne, G., & Kraus, A. 2013, ARA&A, 51, 269, doi: [10.1146/annurev-astro-081710-102602](https://doi.org/10.1146/annurev-astro-081710-102602)
- Duchêne, G., & Kraus, A. 2013, Annual Review of Astronomy and Astrophysics, 51, 269, doi: [10.1146/annurev-astro-081710-102602](https://doi.org/10.1146/annurev-astro-081710-102602)
- Eggleton, P., & Kiseleva, L. 1995, ApJ, 455, 640, doi: [10.1086/176611](https://doi.org/10.1086/176611)
- Eggleton, P. P., & Tokovinin, A. A. 2008, MNRAS, 389, 869, doi: [10.1111/j.1365-2966.2008.13596.x](https://doi.org/10.1111/j.1365-2966.2008.13596.x)
- . 2010, VizieR Online Data Catalog, J/MNRAS/389/869
- Fernandez, M. A., Covey, K. R., De Lee, N., et al. 2017, PASP, 129, 084201, doi: [10.1088/1538-3873/aa77e0](https://doi.org/10.1088/1538-3873/aa77e0)
- Gaia Collaboration, Brown, A. G. A., Vallenari, A., et al. 2018, A&A, 616, A1, doi: [10.1051/0004-6361/201833051](https://doi.org/10.1051/0004-6361/201833051)
- Gaulme, P., Borkovits, T., Appourchaux, T., et al. 2022, A&A, 668, A173, doi: [10.1051/0004-6361/202244373](https://doi.org/10.1051/0004-6361/202244373)
- Gray, R. O., & Corbally, C. J. 1994, AJ, 107, 742, doi: [10.1086/116893](https://doi.org/10.1086/116893)
- Green, G. M., Schlafly, E., Zucker, C., Speagle, J. S., & Finkbeiner, D. 2019, ApJ, 887, 93, doi: [10.3847/1538-4357/ab5362](https://doi.org/10.3847/1538-4357/ab5362)
- Han, Z., Podsiadlowski, P., Maxted, P. F. L., Marsh, T. R., & Ivanova, N. 2002, MNRAS, 336, 449, doi: [10.1046/j.1365-8711.2002.05752.x](https://doi.org/10.1046/j.1365-8711.2002.05752.x)
- Harrington, R. S. 1977, RMxAA, 3, 139
- Koleva, M., Prugniel, P., Bouchard, A., & Wu, Y. 2009, A&A, 501, 1269, doi: [10.1051/0004-6361/200811467](https://doi.org/10.1051/0004-6361/200811467)
- Kounkel, M., Covey, K. R., Stassun, K. G., et al. 2021, AJ, 162, 184, doi: [10.3847/1538-3881/ac1798](https://doi.org/10.3847/1538-3881/ac1798)

- Kovalev, M., Chen, X., & Han, Z. 2022, *MNRAS*, 517, 356, doi: [10.1093/mnras/stac2513](https://doi.org/10.1093/mnras/stac2513)
- Kummer, F., Toonen, S., & de Koter, A. 2023, arXiv e-prints, arXiv:2306.09400, doi: [10.48550/arXiv.2306.09400](https://doi.org/10.48550/arXiv.2306.09400)
- Kurucz, R. 1993, *SYNTHE Spectrum Synthesis Programs and Line Data*. Kurucz CD-ROM No. 18. Cambridge, 18
- Li, C.-q., Shi, J.-r., Yan, H.-l., et al. 2021, *ApJS*, 256, 31, doi: [10.3847/1538-4365/ac22a8](https://doi.org/10.3847/1538-4365/ac22a8)
- Li, J., Li, J., Liu, C., et al. 2022, *The Astrophysical Journal*, 933, 119, doi: [10.3847/1538-4357/ac731d](https://doi.org/10.3847/1538-4357/ac731d)
- Luo, A. L., Zhao, Y.-H., Zhao, G., et al. 2015, *Research in Astronomy and Astrophysics*, 15, 1095, doi: [10.1088/1674-4527/15/8/002](https://doi.org/10.1088/1674-4527/15/8/002)
- Merle, T., Van Eck, S., Jorissen, A., et al. 2017, *A&A*, 608, A95, doi: [10.1051/0004-6361/201730442](https://doi.org/10.1051/0004-6361/201730442)
- Moe, M., & Kratter, K. M. 2018, *ApJ*, 854, 44, doi: [10.3847/1538-4357/aaa6d2](https://doi.org/10.3847/1538-4357/aaa6d2)
- Nasab, H. H., Pazhouhesh, R., & Roobiat, K. Y. 2023, *NewA*, 103, 102051, doi: [10.1016/j.newast.2023.102051](https://doi.org/10.1016/j.newast.2023.102051)
- Offner, S. S. R., Moe, M., Kratter, K. M., et al. 2022, arXiv e-prints, arXiv:2203.10066, doi: [10.48550/arXiv.2203.10066](https://doi.org/10.48550/arXiv.2203.10066)
- Raghavan, D., McAlister, H. A., Henry, T. J., et al. 2010a, *ApJS*, 190, 1, doi: [10.1088/0067-0049/190/1/1](https://doi.org/10.1088/0067-0049/190/1/1)
- . 2010b, *ApJS*, 190, 1, doi: [10.1088/0067-0049/190/1/1](https://doi.org/10.1088/0067-0049/190/1/1)
- Rappaport, S. A., Borkovits, T., Gagliano, R., et al. 2022, *MNRAS*, 513, 4341, doi: [10.1093/mnras/stac957](https://doi.org/10.1093/mnras/stac957)
- Royer, F., Zorec, J., & Gómez, A. E. 2007, *A&A*, 463, 671, doi: [10.1051/0004-6361:20065224](https://doi.org/10.1051/0004-6361:20065224)
- Tokovinin, A. 2018, *ApJS*, 235, 6, doi: [10.3847/1538-4365/aaa1a5](https://doi.org/10.3847/1538-4365/aaa1a5)
- . 2021, *Universe*, 7, 352, doi: [10.3390/universe7090352](https://doi.org/10.3390/universe7090352)
- Toonen, S., Boekholt, T. C. N., & Portegies Zwart, S. 2022, *A&A*, 661, A61, doi: [10.1051/0004-6361/202141991](https://doi.org/10.1051/0004-6361/202141991)
- Toonen, S., Portegies Zwart, S., Hamers, A. S., & Bandopadhyay, D. 2020, *A&A*, 640, A16, doi: [10.1051/0004-6361/201936835](https://doi.org/10.1051/0004-6361/201936835)
- Virtanen, P., Gommers, R., Oliphant, T. E., et al. 2020, *Nature Methods*, 17, 261, doi: [10.1038/s41592-019-0686-2](https://doi.org/10.1038/s41592-019-0686-2)
- Wang, R., Luo, A. L., Chen, J.-J., et al. 2020, *ApJ*, 891, 23, doi: [10.3847/1538-4357/ab6dea](https://doi.org/10.3847/1538-4357/ab6dea)
- Wang, S., & Chen, X. 2019, *ApJ*, 877, 116, doi: [10.3847/1538-4357/ab1c61](https://doi.org/10.3847/1538-4357/ab1c61)
- Wilson, O. C. 1941, *ApJ*, 93, 29, doi: [10.1086/144239](https://doi.org/10.1086/144239)
- Wu, Y., Du, B., Luo, A., Zhao, Y., & Yuan, H. 2014, in *Statistical Challenges in 21st Century Cosmology*, ed. A. Heavens, J.-L. Starck, & A. Krone-Martins, Vol. 306, 340–342, doi: [10.1017/S1743921314010825](https://doi.org/10.1017/S1743921314010825)
- Wu, Y., Luo, A. L., Li, H.-N., et al. 2011, *Research in Astronomy and Astrophysics*, 11, 924, doi: [10.1088/1674-4527/11/8/006](https://doi.org/10.1088/1674-4527/11/8/006)
- Xia, F., Fu, Y., & Wang, X. 2019, *ApJ*, 882, 147, doi: [10.3847/1538-4357/ab32de](https://doi.org/10.3847/1538-4357/ab32de)
- Zhang, B., Liu, C., & Deng, L.-C. 2020, *ApJS*, 246, 9, doi: [10.3847/1538-4365/ab55ef](https://doi.org/10.3847/1538-4365/ab55ef)
- Zhang, B., Li, J., Yang, F., et al. 2021, *ApJS*, 256, 14, doi: [10.3847/1538-4365/ac0834](https://doi.org/10.3847/1538-4365/ac0834)